Palaeogeography, Palaeoclimatology, Palaeoecology 537 (2020) 109413

Contents lists available at ScienceDirect

Palaeogeography, Palaeoclimatology, Palaeoecology

journal homepage: www.elsevier.com/locate/palaeo

Magnetostratigraphic constraints on the age of the *Hipparion* fauna in the Linxia Basin of China, and its implications for stepwise aridification

Weilin Zhang[a,b,*], Xiaomin Fang[a,b], Chunhui Song[c], Maodu Yan[a,b], Jiuyi Wang[d], Zhigao Zhang[e], Fuli Wu[a,b], Jinbo Zan[a,b], Tao Zhang[a], Yibo Yang[a], Mengqi Tan[a]

[a] CAS Key Laboratory of Continental Collision and Plateau Uplift, Institute of Tibetan Plateau Research, Chinese Academy of Sciences, Beijing, 100010, China
[b] CAS Center for Excellence in Tibetan Plateau Earth Sciences, Chinese Academy of Sciences (CAS), Beijing, 100101, China
[c] School of Earth Sciences & Key Laboratory of Western China's Mineral Resources of Gansu Province, Lanzhou University, Lanzhou, 730000, China
[d] MLR Key Laboratory of Metallogeny and Mineral Assessment, Institute of Mineral Resources, Chinese Academy of Geological Sciences, Beijing, 100037, China
[e] School of Resource Environment and Tourism, Anyang Normal University, Anyang, Henan, 455000, China

ARTICLE INFO

Keywords:
Magnetostratigraphy
Hipparion
Late miocene
Aridification
Linxia basin

ABSTRACT

Late Cenozoic sediments in the Linxia Basin of China, on the northeastern Tibetan Plateau, bear abundant fossils of the *Hipparion* fauna. From late Miocene times, these sections record a history of aridification in the Asian Interior, the evolution of the east Asian monsoon, and multiple uplifts of the Tibetan Plateau. In this paper, a new detailed magnetostratigraphic study of a sedimentary sequence from the Duikang (DK) section containing the *Hipparion* fauna is presented, to better understand interconnected ecologic and environmental changes. The 90-m-thick section reveals nine normal and nine reversed zones that span from chron. C5n.2n to chron. C3Ar or from chron. C4n.2n to chron. C2Ar, yielding magnetostratigraphic ages of ~8.1 Ma - 3.7 Ma for the studied section and 5.3 Ma for the *Hipparion* fauna-bearing bed. Combined with all the previous magnetostratigraphic ages of the fauna-bearing sediments in the Linxia Basin, *Hipparion* can be distinguished as mainly having lived during five periods: Phase I (11.5 Ma), Phase II (8.2 Ma), Phase III (6.3 Ma), Phase IV (~5.3 Ma) and Phase V (2.5 Ma). Based on comparison of climate records in the Linxia Basin with aridification records from surrounding regions and global cooling during the late Cenozoic, we suggest that the evolution of *Hipparion* from the Linxia Basin was mainly driven by continuous global cooling and tectonic uplift of the northeastern Tibetan Plateau since the late Miocene.

1. Introduction

Hipparion was widely distributed in North America and the Old World between the late Miocene and Pliocene and is an important biomarker for stratigraphic correlations and environmental reconstructions (Macfadden, 1984; Alberdi, 1989; Qiu et al., 1987; Fang et al., 2003; Deng et al., 2013a; Zhang et al., 2019). Environmental changes and continental connections in the Late Miocene triggered the *Hipparion* to migrate across the Bering land bridge to the Eurasian continent and further into China (Woodburne and Swisher, 1995; Bernor et al., 1996); their fossils can be observed in the late Cenozoic basins in the Tibetan Plateau and the red-clay deposits in northern China (Qiu et al., 2013; Deng et al., 2015, 2019) (Fig. 1A). *Hipparion* experienced long-term continuous evolutions from the early Eocene *Hyracotherium* to the Quaternary *Proboscidipparion* and *Equus* due to changes in the global climate and the regional ecologic environment (Fig. 2). The Linxia Basin in the northeastern Tibetan Plateau is a closed basin that contained an abundant terrestrial water system during the late Miocene and became an ideal habitat for the *Hipparion* (Fang et al., 2003; Zhang et al., 2019) (Fig. 1A). At present, innumerable fossils of the *Hipparion* fauna have been collected at dozens of sites by paleontologists from the Institute of Vertebrate Paleontology and Paleoanthropology, Chinese Academy of Sciences (Fig. 3). Previous studies of the Linxia Basin mainly focused on the paleoclimate change, the tectonosedimentary evolution of the fluviolacustrine sequence (Dettman et al., 2003; Fang et al., 2003, 2016; Fan et al., 2006) and the species identification of the mammals (Deng, 2004; Deng et al., 2004, 2013a; Qiu et al., 2013; Wang et al., 2013). *Hipparion* in the Linxia Basin was buried at different sedimentary beds from different periods (Wang et al., 2010; Deng et al., 2013a; Fang et al., 2003, 2016; Zan

* Corresponding author. CAS Key Laboratory of Continental Collision and Plateau Uplift, Institute of Tibetan Plateau Research, Chinese Academy of Sciences, Beijing, 100010, China.
E-mail address: zhangwl@itpcas.ac.cn (W. Zhang).

https://doi.org/10.1016/j.palaeo.2019.109413
Received 28 May 2019; Received in revised form 10 October 2019; Accepted 16 October 2019
Available online 19 October 2019
0031-0182/

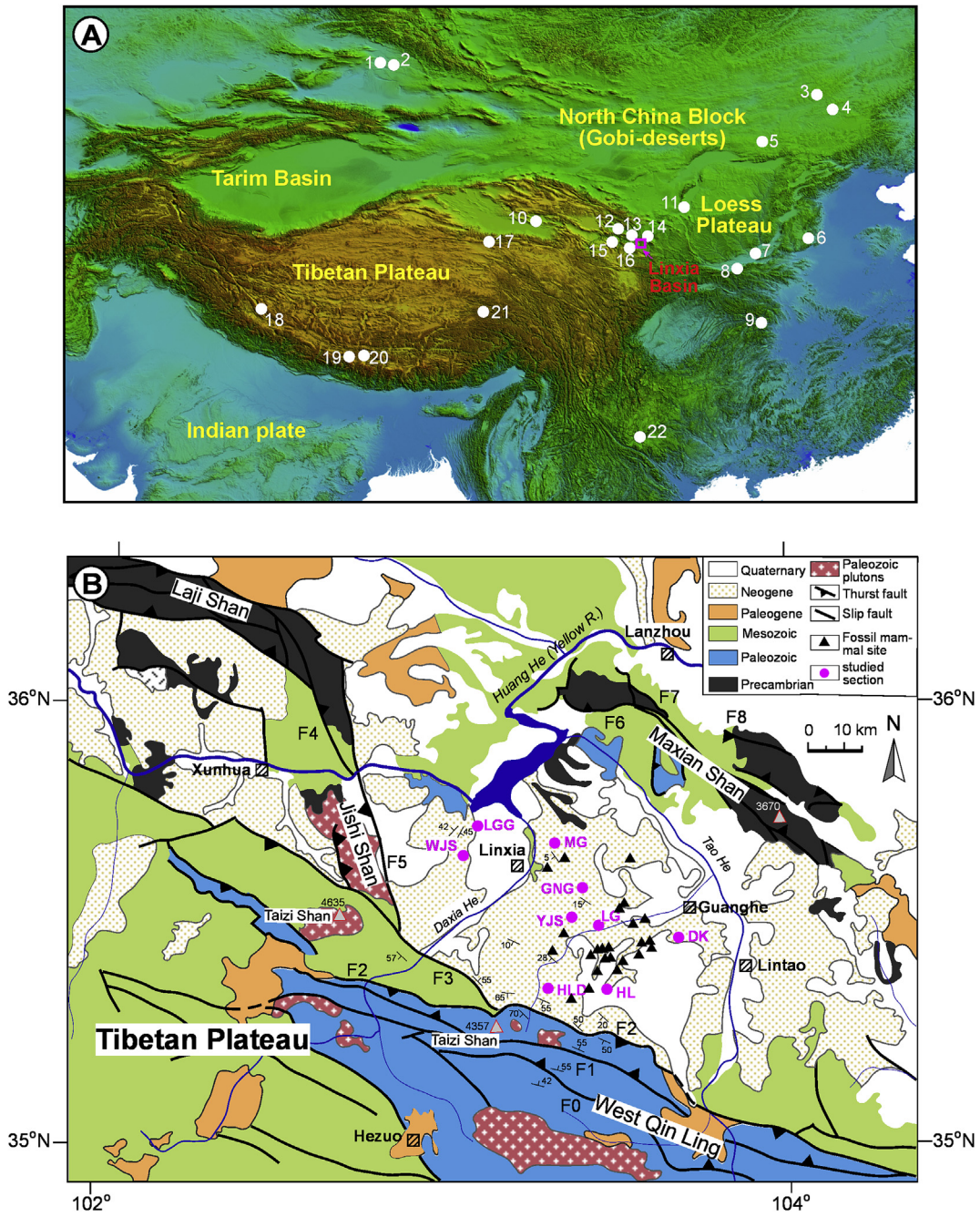

Fig. 1. (A) Distribution of sites with *Hipparion* in China (cited from Qiu et al., 2013; Deng et al., 2015, 2019) and the location of the Linxia Basin in the NE Tibetan Plateau with respect to the Loess Plateau and the Tibetan Plateau; 1–2: northern Junggar Basin, 3-4-5: middle part of Inner Mongolia, 6: Yushe in Shanxi Province, 7: Xinxiang in Henan Province; 8: Lantian in Shanxin Province; 9: Fangxian in Hubei Province, 10: Qaidam Basin, 11: Tongxin in the Ningxia region, 12: Xining Basin, 13: Minhe Basin, 14: Lanzhou Basin, 15: Guide Basin, 16: Xunhua Basin, 17: Kunlun Pass Basin, 18: Zanda Basin, 19: Jilong-Woma Basin, 20: Dati Basin, 21: Xiaquka-Bulong Basin, and 22: Xiaolongtan Basin. (B) Geologic map of the Linxia Basin showing the distribution of the Cenozoic stratigraphy and its surrounding tectonic units and major faults. DK-Duikang section, GNG-Guonigou secyion, HLD-Heilinding section, HL-Hualin section, LG-Laogou section, LGG-Longguang section, MG-Maogou section, WJS-Wangjiashan section, YJS-Yangjiashan section.

et al., 2016; Zhang et al., 2019), indicating its long-term environmental adaptation and continuous evolution since the late Miocene. However, the evolutionary processes and survival ages of the *Hipparion* fauna are still a controversial subject due to a lack of precise age dating of the long continuous sequence of fluviolacustrine sediments bearing the fossils of the *Hipparion* fauna.

The *Hipparion* fauna in the Linxia Basin was mainly discovered in the red fluvial-lacustrine siltstones or mudstones, including the perissodactyla, artiodactyla and carnivora fossils. The emergence, evolution and extinction of these mammals, which are relatively sensitive to environmental changes, are closely related to the evolution of aridification and the east Asian monsoon (Qiu et al., 2013; Fang et al., 2016; Zan et al., 2016). To support and enhance the understanding of the regional environmental evolution associated with the Asian monsoon evolution and the uplift of the Tibetan Plateau, obtaining the accurate survival ages of the mammals in the Linxia Basin would represent a key breakthrough. In this paper, we present a detailed magnetostratigraphic analysis of a 90 m thick Duikang (DK) section bearing *Hipparion* fauna. We then combined the results from all the previous magnetostratigraphic ages with *Hipparion* in the Linxia Basin

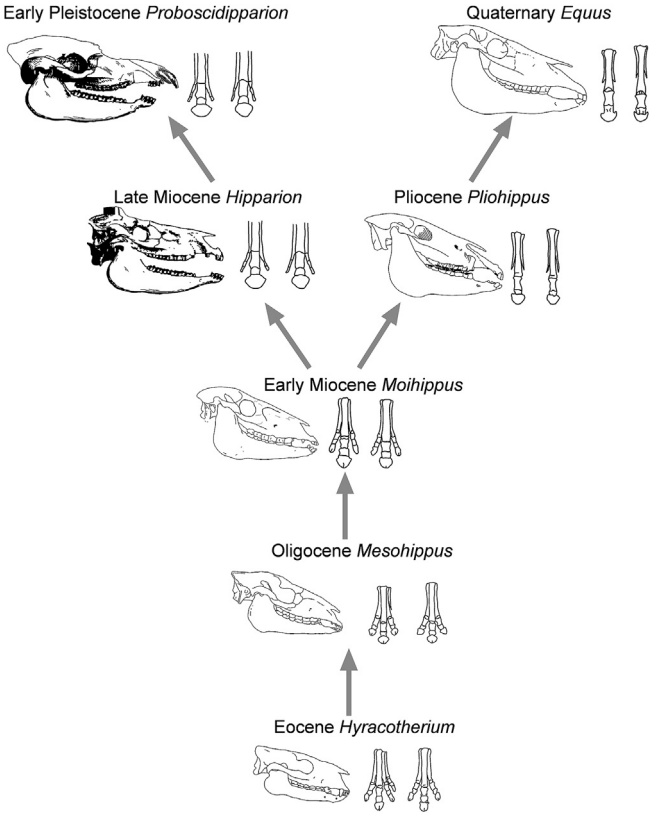

Fig. 2. Evolution of horses including skulls, front-toes and rear-toes plotted from left to right (their contours are modified from Tong, 2002).

to provide its precise chronology and to shed light on the evolutions of Asian aridification and monsoon and the living environments of *Hipparion* since the late Miocene.

2. Geological and biostratigraphic setting

The Linxia Basin, with length of 200 km and width of 75 km, lies on the northeastern margin of the Tibetan Plateau and on the western margin of the Chinese Loess Plateau and has an average elevation of approximately 1800–2600 m surrounded by the mountains with elevations of approximately 3000–4000 m (Fig. 1A). Linxia Basin is an intracontinental flexural (foreland) basin (Fang et al., 2003, 2016; Li et al., 2014) controlled by the W-E trending West Qin Ling fault and the N–S trending Jishi Shan fault (Fig. 1B). The Cenozoic basin strata have great lateral variations of thickness and sedimentary facies from the margin of the mountain to the center of the basin, as verified by the magnetostratigraphic ages (Li et al., 1995, 1997; Fang et al., 2003, 2016; Zhang et al., 2019). The differences of sediments and sedimentary thickness in different localities from the basin have led to confusion regarding stratigraphic divisions using the biostratigraphy of the fossilized mammals.

The Cenozoic stratigraphy of the Linxia Basin consists mainly of red beds of fluvio-lacustrine mudstones and siltstones in its center, and thick strata of gray to reddish-brown conglomerates and sandstones on its margins. The sedimentary sequence since the late Miocene is primarily composed of the late Miocene Dongxiang Fm. and Liushu Fm. with red siltstone and mudstone, the Early and Late Pliocene Hewangjia Fm. with yellowish - brown calcareous mudstone and Jishi Fm. or Jishi Conglomerate Bed (Li et al., 1995, 1997; Fang et al., 2003, 2016), and loess deposits during the Quaternary (Zan et al., 2016, 2018). The *Hipparion* fauna was mainly found in the upper Dongxiang Fm., the entire Liushu Fm. and the early Quaternary loess (Deng et al., 2004; Zan et al., 2016; Zhang et al., 2019). The oldest *Hipparion* fauna was excavated from the GNG section and the WJS section (WJS) (for their site, see Fig. 1B) dated at 11.5 Ma (Fang et al., 2003, 2016), and its species mainly include *Hipparion donxiangense, Parelasmotherium linxiaense, Dinocrocutu gigantea, Machairodus* sp., *Tetralophodon* sp., *Shaanxispira* sp., *Pararhizomys hipparionum, Promephitis parvus, Ictitherium* sp., *Hyaenictitherium wongii, Dinocrocuta gigantea, Tetralophodon* sp., *Hipparion* sp., *Acerorhinus hezhengensis, Chilotherium wimani, Chleuastochoerus stehlni,* and *Miotragocerus* sp. (Fang et al., 2003; Deng et al., 2013a) (Fig. 3). The Liushu Fm. contains the *Hipparion* faunas from two different periods (Deng et al., 2004; Fang et al., 2003), i.e., *Hipparion* sp., *Chilotherium* sp., *Honanotherium* sp., *Cervavitus* sp., *Protalactaga* cf. *tunggurensis, Spalacinae gen. indet., Castoridaegen indet., Ochotona lagrelii minor, Ictitherium hipparionum hyaenoides, Adcrocuta* cf. *eximia variabilis* in the lower-middle Liushu Fm. from the WJS section (Gu et al., 1995; Fang et al., 2003), *Hystrix gansuensis, Promephitis* sp., *Pleisiogulo* sp., *Ictitherium* sp., *Hyaenictitherium wongii, H. hyaenoides, Adcrocuta variabilis, Machairodus* sp., *Metailurus* sp., *Felis* sp., *Hipparion* sp., *Chilotherium wimani, Chleuastochoerus stehlini, Parataxidea sinensis, Hipparion coelophyes, H. dermatorhinum, Acerorhinus hezhengensis, Dicerorhinus ringstromi, Ancylotherium* sp., *Microstonyx major, Metacervulus* sp., *Honanotherium schlosseri, Palaeotragus microdon, Miotragocerus* sp., *Sinotragus* sp., *Protoryx* sp., and *Gazella* sp. in the upper Liushu Fm. from the LG, LGG, HLD, HL, MG, WJS sections (for the sites, see Fig. 1B) (Fang et al., 2003; Wang et al., 2010; Zhang et al., 2019). These two *Hipparion* types from the Liushu Fm. are correlated to the MN 11 and MN 12/13 of the European mammal zones and the Baodean of biochronology in China (Steininger, 1999; Deng et al., 2013a), and are also verified by the ages of ~8.2 Ma and ~6.3 Ma from paleomagnetic dating (Fang et al., 2003, 2016; Wang et al., 2010; Zhang et al., 2019) (Fig. 3). The *Hipparion* fauna during the early Pliocene is found in the Hewangjia Fm. from the WJS and DK sections, chiefly comprising *Hipparion* sp., *Hystrix gansuensis, Alilepus* sp., *Promephitis* sp., *Chasmaporthetes* sp., *Hyaenicyitherium wongii, Cervavitus novorossiae, Palaeotragus* sp., *Samotherium* sp., *Protoryx* sp., *Capricornis* sp., and *Sinotragus* sp. (Deng et al., 2011; Fang et al., 2003) (Fig. 3). The youngest *Hipparion* fauna from the LD section is buried in the loess deposits and mainly contains *Hipparion (Proboscidipparion) sinense, Aepyosciurus orientalis, Marmota parva, Castor* sp., *Mimomys* cf. *gansunicus, Bahomys* sp., *Sericolagus brachypus, Macaca* cf. *anderssoni, Paradolichopithecus gansuensis, Vulpes chikushanensis, Canis teilhardi, C. longdanensis, C. brevicephalus, Sinicuon* cf. *dubius, Eirictis robusta, Meles teilhardi, Chasmaporthetes progressus, Pachycrocuta licenti, Crocuta honanensis, Homotherium crenatidens, Megantereon nihowanensis, Sivapanthera linxiaensis, Pantherapalaeosinensis, Felis teilhardi, Lynx shansius, Equus eisenmannae, Coelodonta nihowanensis, Hesperotherium* sp., *Sus* sp., *Nipponicervus longdanensis, Gazella* cf. *blacki, Leptobos brevicornis,* and *Hemibos gracilis* (Qiu et al., 2004; Deng et al., 2012, 2013a; Bernor and Sun, 2015; Zan et al., 2016). In this study, magnetostratigraphy is applied to the DK section to study the *Hipparion* fauna, and all the previous magnetostratigraphic studies are compiled for a comprehensive correlation to estimate the survival ages of *Hipparion* in the Linxia Basin.

3. Sampled section

The 90 m-thick DK section (35°25′23.4″N, 103°32′55.3″E, 2145 m asl) is located 6.5 km southwest of Guanghe County (Fig. 1B). The area is unconformably covered by the late Pleistocene Malan loess, and bedding is approximately horizontal (Fig. 4C). The depositional sequence from the DK section is mainly characterized by fine grain sediments with brown-red mudstones and siltstones. The lower part of the section (0–55 m) contains mainly thick brown-red paleosol complexes and mudstones intercalated with thin multilayers of coarse sandstones (Fig. 4B, C). Although the paleosol complexes are weakly developed, the Bt horizon (granular argillic layer) and the Bk horizon (carbonate nodule layer) are still easily distinguished from the whole beds

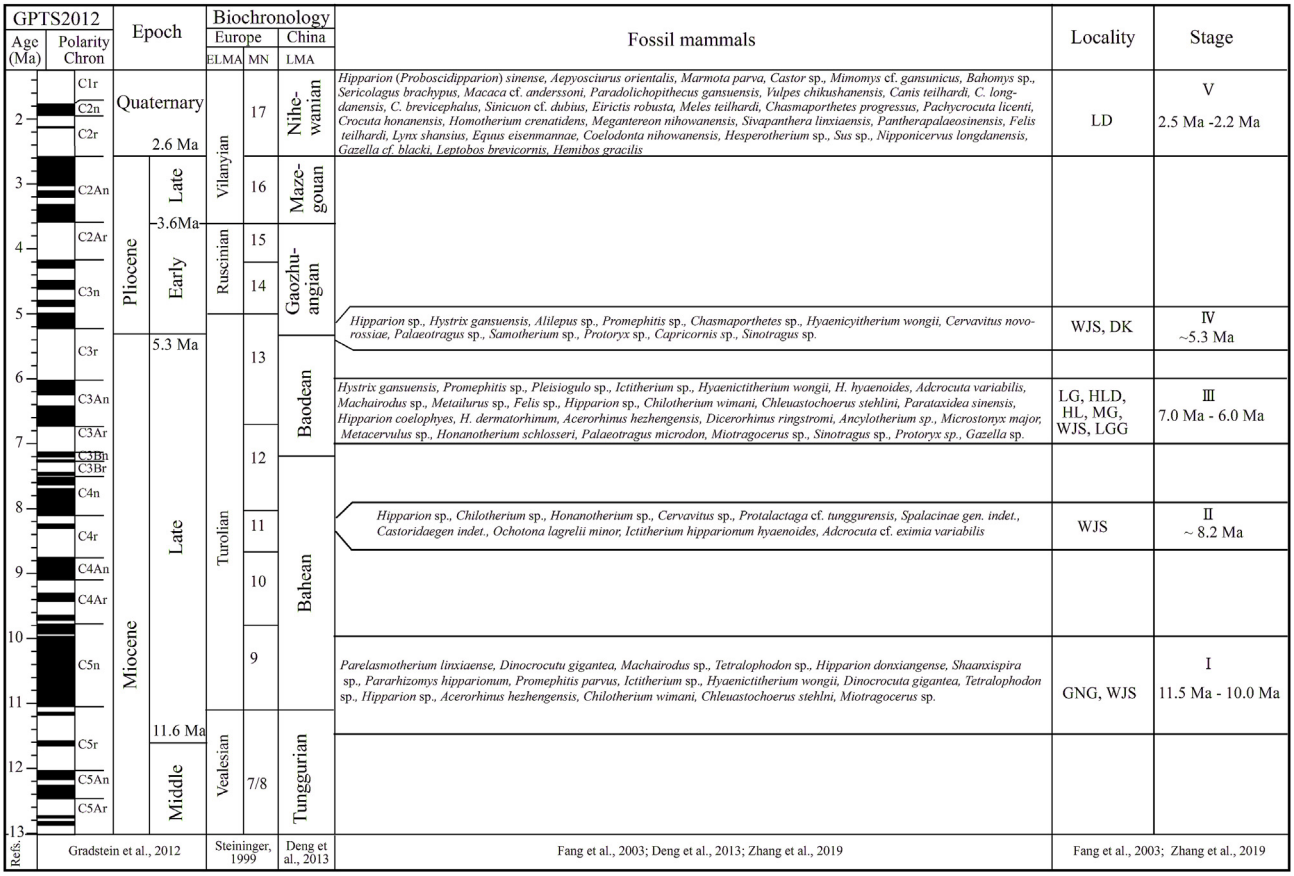

Fig. 3. Fossilized mammals from the *Hipparion* fauna found in the Linxia Basin (Deng et al., 2013) and their corresponding ages and locations (Fang et al., 2003; Zhang et al., 2019).

(Fig. 4C). The Bt horizon has a thoroughly granular ped structure, clay illuviation and carbonate depletion. The grayish-light brown carbonate Bk horizon was developed under the Bt horizon, with many small white and gray carbonate nodules, coatings and infillings (Fig. 4C). The upper part of the section (55–90 m) consists of brownish - yellow mudstones consisting of many calcareous nodules and light brown calcic mudstones (Fig. 4D), and its bottom is grayish-light brown sandstone and sandy conglomerate beds (Fig. 4E). The *Hipparion* fauna is just found in this sandy conglomerate bed with a thickness of 57–59 m, and the observed species include Rodentia (*Hytrix gansuensis*), Lagomorpha (*Alilepus* sp.), Carnivora (*Sinictis dolichognathus, Parataxidea sinensis, Hyaenictitherium wongii, Adcrocuta eximia, Chasmaporthetes kani* and *Flis* sp.), Perissodactyla (*Hipparion hippidiodus, H. platyodus, H. licenti, H. (Proboscidipparion) pater, Shansirhinus ringstroemi, Hesperotherium* sp. and *Ancylotherium* sp.), and Artiodactyla (*Cervavitus novorossiae, Palaeotragus microdon, Samotherium* sp., *Sinotragus* sp. and *Gazella blacki*) (Deng et al., 2011). These 20 mammal species appeared during the Gaozhuangian stage of biochronology in China or mainly during the late Miocene (Deng et al., 2011), but no magnetostratigraphic age constraints have been performed on the sediments of this section for verification.

4. Sampling and measurements

The DK section was cut into an gully by surface runoff, the most sedimentary sequence was exposed while a very small part of the section was covered by weathering materials or aeolian loess (Fig. 4). In this study, all the samples were taken by digging 0.5–1 m deep pits into the original beddings, the total of 326 oriented block samples from the DK section were collected at 0.25 m stratigraphic intervals within the siltstone and mudstone beds and 0.5–1 m intervals in the beds between 16 m and 62 m with thin sandstone layer or sandy conglomerate layer, and the lenses of mudstones or siltstones were evaluated. All paleomagnetic block samples were oriented in the field using a magnetic compass. Each block sample was cut into three sets of 2 × 2 × 2 cm cubic subsamples in the laboratory, forming three parallel sets of samples for cross-calibration measurements.

Ten powdered samples from different layers were selected to measure their low-field temperature-dependent magnetic susceptibility (κ-T) runs in a MFK1-FA Kappabridge equipped with a CS-4 high-temperature furnace (Agico Ltd., Brno, Czech Republic). These corresponding oriented samples were conducted by stepwise thermal demagnetizations in nineteen steps between room temperature and 690 °C on a 2G Enterprises Model 755 cryogenic magnetometer at the Institute of Tibetan Plateau Research, Chinese Academy of Sciences, in a magnetically shielded room (< 150 nT). For all the paleomagnetic specimens, the thermal demagnetizations with nine discrete steps above 400 °C were performed on a 2G Enterprises He-free u-channel SQUID magnetometer (2G-755R) at the Department of Geosciences, Tübingen University, Germany.

Representative thermal demagnetization diagrams show most samples have a rapid decrease in remanence intensity between 500 °C and 580 °C (Fig. 5A), linearly pointing toward the origin above 450 °C (Fig. 5B) and reaching the minimum at 690 °C. Only few samples reveal two magnetic components, i.e., a low-temperature component (LTC) and a high-temperature component (HTC). The remanence intensity of the LTC usually gradual increase at temperatures less than 300 °C (Fig. 5A), the HTC reveals a stable demagnetization at 585 °C and points to the origin at 690 °C in the orthogonal plot (Fig. 5B). Thus, we suggest that magnetite and hematite are the carriers of the Characteristic Remanent Magnetization (ChRM). Similarly, the κ-T curves have a sudden decrease in susceptibility at ~580 °C and attain a minimum value at

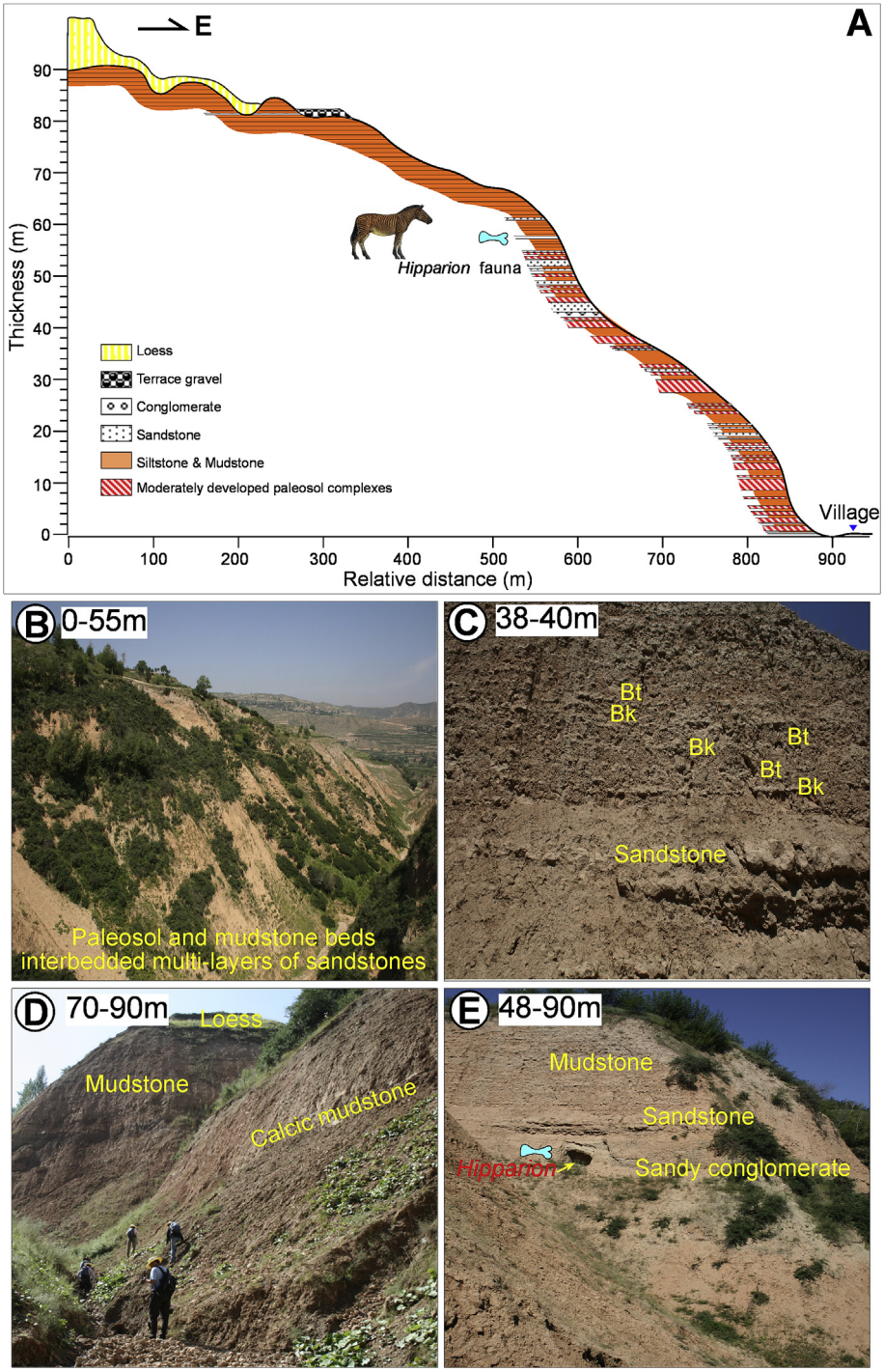

Fig. 4. (A) Geologic cross profile showing the stratigraphic successions of the Duikang section; (B) photo showing the sedimentary sequence of paleosol complexes and mudstones intercalated with multilayers of coarse sandstones in the lower section; (C) photos showing clear luvic Bt and calcic Bk horizons; (D) photo showing the sedimentary sequence of mudstones consisting of calcareous nodules and calcic mudstones in the upper section; (E) photo showing the sandstone and sandy conglomerate beds bearing the *Hipparion* fauna.

690 °C (Fig. 5C), also indicating the existences of magnetite and hematite. The characteristics of these remanant minerals are consistent with the original rock magnetic analysis from the other sections in the Linxia Basin (Wang et al., 2010; Fang et al., 2016; Wu et al., 2017; Zhang et al., 2019).

The characteristic remanent magnetization (ChRM) directions were determined by nine steps of the thermal demagnetization path above ~400 °C using principal component analysis. A group of 254 samples from the 326 total samples attained reliable ChRM directions. The virtual geomagnetic polarity (VGP) latitudes were calculated from the ChRM directions of the 254 samples.

5. Magnetostratigraphic result

The ChRM directions from the DK section yield a mean normal direction of D/I = 3.2°/47.5° (k = 6.0, α_{95} = 5.4°, n = 141), and a mean reversed direction of D/I = 179.6°/-41.2° (k = 8.0, α_{95} = 7.6°, n = 113) (Fig. 6a) in geographic coordinates. The means of the reversed

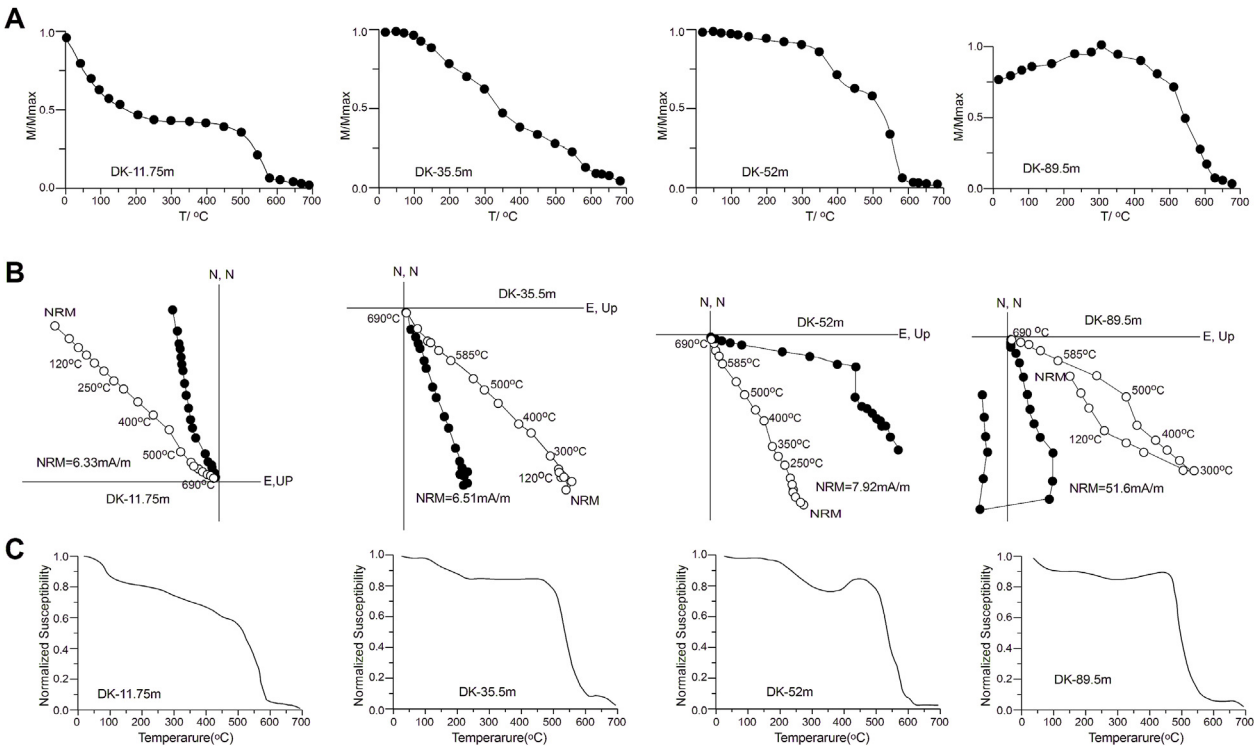

Fig. 5. (A) Remanence intensity versus temperature for the thermal demagnetization of the NRM; (B) orthogonal vector plots of thermal demagnetization; open (closed) symbols represent vertical (horizontal) projections; (C) high-temperature magnetic susceptibility (κ-T) curves.

and normal modes are not distinguishable at the 95% level of confidence, indicating a positive reversal test with classification B (Tauxe, 1998; McFadden and McElhinny, 1990). The Gaussian distribution of the ChRM vectors from a statistical bootstrap technique (Tauxe, 1998) demonstrates that the bootstrap reversal test is also positive (Fig. 6b). Therefore, we believe that the obtained ChRM directions from the DK section are likely primary and reliable magnetizations.

The VGP-latitudes along with the stratigraphic position were applied to the establishment of the final magnetic polarity intervals of the sedimentary sequence from the DK section. Each polarity zone was determined by at least two successive data points of the same ChRM polarity, and a total of nine normal and nine reversed polarity zones

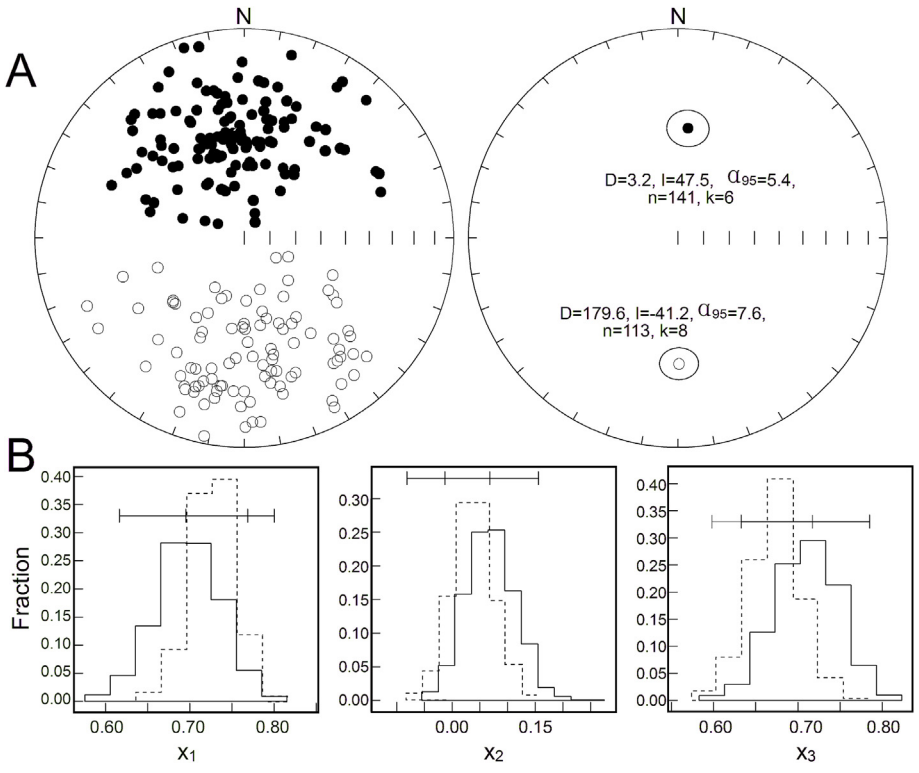

Fig. 6. (A) Equal-area projections of the ChRM directions and mean directions (with 95% confidence limits) for the DK section. α_{95}, N and k are, respectively, the 95% confidence limit, the number of samples and the precision parameter. (B) Histograms of Cartesian coordinates of bootstrapped means of para-data sets of the DK section.

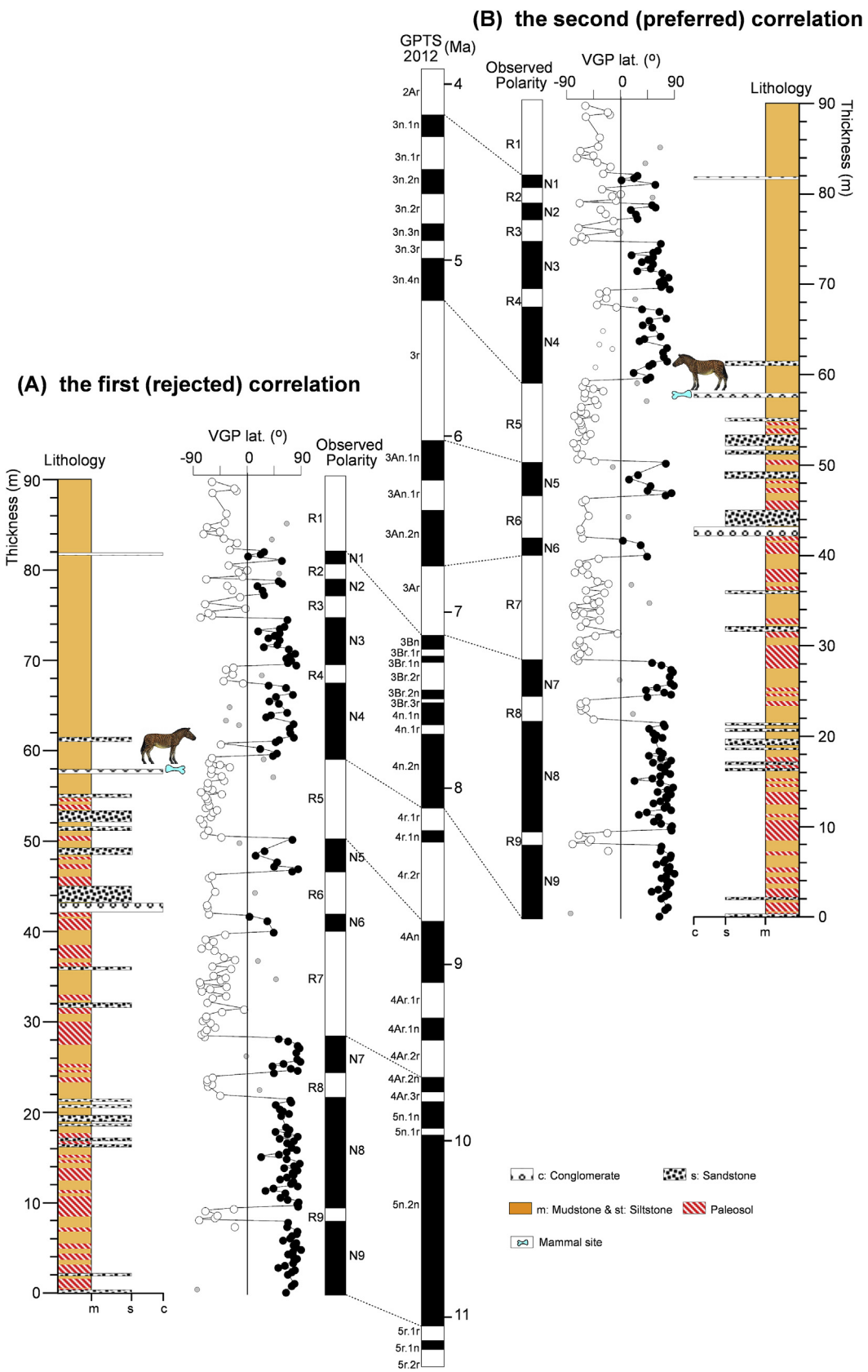

Fig. 7. Magnetostratigraphy of the DK section and its two correlations with the geomagnetic polarity time scale (GPTS) of Gradstein et al. (2012). Small gray open/closed circles represent single opposite samples within the multiple successive data points from one polarity zone.

designated as N1–N9 and R1-R9, respectively, were identified (Fig. 7). Our observed polarity zones (N1–N9 and R1-R9) from the entire DK section provided two possible correlations with the geomagnetic polarity time scale (GPTS) (Gradstein et al., 2012) as follows: 1) the first correlation with chrons. C5n.2n - C3Ar (Fig. 7A), i.e., the top and strikingly long reverse interval R1 is correlated with the long predominantly reverse polarity chron. C3Ar, the short normal intervals N1 and R1 and the short reverse interval R2 can be matched to chrons. C3Bn, C3Br.1r and C3Br.1n; the two long normal polarity intervals N3 and N4 and the two short reverse intervals R3 and R4 are matched to chrons. C3Br.2n, C3Br.3r, C4n.1n, C4n.2n, C3Br.2r and C4n.1r; the notable long reverse intervals R5, R6, R7 and the short normal intervals N5, N6 are closely matched to chrons C4r.1r-C4r.1n-C4r.2r, C4Ar.1r, C4Ar.2r, C4An and C4Ar.1n; the three intervals N7, N8 and N9 and the two short reverse intervals R8 and R9 at the bottom are together matched to the chrons. from C4Ar. 2n to C5n.2n; 2) the second correlation with chrons. C4n.2n - C2Ar (Fig. 7B), i.e., the four reverse intervals R1, R2, R3, R4 and four normal intervals N1, N2, N3, N4 from the upper part of the section are highly correlated with chrons. C2Ar, the three reverse polarity chrons. and the four normal polarity chrons. within chron. C3n; the reverse intervals R5, R6, R7 and the normal intervals N5, N6 in the middle part of the section are correlated with chrons. C3r, C3An.1r, C3Ar, C3An.1n and C3An.2n; the N7, N8, N9 and the R8, R9 at the lower part of the section are together correlated with chrons. C3Bn to C4n.2n.

From the thickness versus age distribution of polarity changes, the sedimentation rate (SR) was calculated from the major polarity chrons. of our two interpreting correlation models (Fig. 8). The two curves (red and blue) of the thickness versus age are almost parallel, and the values of the SRs are almost all within the range from 15 cm/kyr to 25 cm/kyr (Fig. 8); this is a small variation and is close to the SR of Miocene red clay (~17.0 cm/kyr) (Guo et al., 2002), the SR of late Miocene - early Pliocene red clay (~21.0 cm/kyr) (Hao and Guo, 2004) and the SR of Oligocene – Pliocene fluvial-alluvial red beds (~17.5 cm/kyr) (Fang et al., 2003, 2016). Although the SRs calculated by these two correlation models with GPTS 2012 cannot be easily applied to distinguish the optimal correlation, the stratigraphy of the DK section can clearly be divided into the late Miocene Baodean stage and the early Pliocene Gaozhuangian stage; their boundary is at 0.8 m below the fossil mammalian bed based on the coexistence of the mammalian species from the late Miocene and the early Pliocene (Deng et al., 2011). In applying the previous paleomagnetic results from the MG section to the stratigraphic correlations (Li et al., 1995; Fang et al., 2003), the fossil-bearing horizon should be correlated to chron. C3n.4n with an age of 5.0 Ma corresponding to MN 14 of the European mammal zones (Deng et al., 2011). Following the robust age constraints of this bed containing the fossil mammals, we suggest that the second correlation is the optimal choice, thereby indicating that the sedimentary sequence in the DK section was deposited between ~8.1 Ma and 3.7 Ma, and the *Hipparion* fauna at the level of 57–59 m appeared at 5.3 Ma (Fig. 7B).

6. Discussion

6.1. Magnetostratigraphic ages of the Hipparion fauna in the Linxia Basin

As an intracontinental foreland basin, the stratigraphy in the Linxia Basin are difficult to be laterally correlated (Fang et al., 2016; Zhang et al., 2019), which lead to misdetermination of stratigraphic ages and miscorrelation of the stratigraphic formations (Fang et al., 2016). In the past decades, many well-exposed outcrop sections and deep drillings had been conducted on the paleomagnetic age studies (Li et al., 1997; Fang et al., 1997, 2003; 2016; Wang et al., 2010; Wu et al., 2017; Zan et al., 2016, 2018; Zhang et al., 2019). All these previous studied sections/drillings contain abundant mammalian fossils and comprised the continuous and complete sedimentary sequence, and achieved their accurate and reliable paleomagnetic ages, which will provide a favorable opportunity for further study the chronologies of the *Hipparion* fauna.

The *Hipparion* fauna in the Linxia Basin exists at different horizons in the different sites (Deng et al., 2013a; Fang et al., 2003, 2016; Zhang et al., 2019) due to the shift of the depocenter and the variations in deposition thickness and lithology during the foreland basin evolution (Fang et al., 2016), indicating the *Hipparion* fauna experienced multistage evolutions since the late Miocene. Based on the morphological characteristics of limbs, phalanges and cheek teeth from three toed horses, such as *Hipparion dongxiangense, H. weihoense* and *H. Chiai,* the earliest *Hipparion* fauna was designated as appearing in the early Late-Miocene (Qiu et al., 1987; Deng et al., 2013b). The observed polarity zones of the GNG section suggested that the short normal interval N5 at the thickness of 100 m within the Dongxiang Fm. was correlated with chron. C5r.2n; this yields an age of 11.5 Ma (designated as Phase I) for the lowermost level of the oldest Chinese *Hipparion* fauna (Fang et al., 2016) (Fig. 9B), which is similar to the horizon of the *Hipparion* fauna in the Qaidam Basin and corresponds to the lower part of MN 9 of the European mammal zones (Deng and Wang, 2004; Qiu and Qiu, 1990; Qiu et al., 1999).

The fossilized mammals at the fourth horizon from top to bottom in the WJS section (for the site see Fig. 1B) are defined as the *Hipparion* fauna of Phase II, which is approximately correlated with the Turolian (5.2 Ma - 9.0 Ma) of the European mammal zones and chron. 4n of the GPTS (Fang et al., 2003; Gu et al., 1995) (Figs. 2 and 9F). Most of the fossil assemblages during this period were found in the lower part of the Liushu Fm. with its bottom age of 10 Ma - 8 Ma (Fang et al., 2016; Zhang et al., 2019), so we suggest that the age of the Phase II *Hipparion* fauna is more reasonable at ~8.2 Ma.

The Phase III *Hipparion* fauna has the widest distribution and is the most abundant species in the Linxia Basin (Fig. 3), and its fossils were found in the LGG section, the WJS section, the MG section, the HLD section, the LG section and the HL section (for their sites see Fig. 1B). Paleomagnetic results for the WJS section and the MG section show that the horizon of the *Hipparion* fauna during this period was correlated to chron. C3An.1n with ~6.3 Ma (Li et al., 1995; Fang et al., 1997, 2003, 2013) (Fig. 9F). Similarly, the Phase III *Hipparion* fauna was dated at ~6.4 Ma within C3An.1r in the LG section (Zhang et al., 2019) (Fig. 9D) and was estimated at ~6.3 Ma in the Heilinding section (Wang et al., 2010; Fang et al., 2016) (Fig. 9G).

In Phase IV, the *Hipparion* fauna fossils were found in the red clays of the Hewangjia Fm. from the WJS section (Li et al., 1995; Fang et al., 2003). The sedimentary sequence of the Hewangjia Fm. includes the boundary between the late Miocene and the early Pliocene, corresponding to the Baodean and Gaozhuangian stages of biochronology in China and MN 13/14 of the European mammal zones (Deng et al., 2011); these zones were dated between ~6 Ma and 4.34 Ma in the MG and WJS sections (Fang et al., 2003) (Fig. 9F) and between 6.5 Ma and 4.1 Ma in the HLD section (Wang et al., 2010; Fang et al., 2016) (Fig. 9G). The ages of the Hewangjia Fm. provided approximate constraints for the Phase IV *Hipparion* fauna with an age of ~4.8 Ma (Fang et al., 2003) (Fig. 9F), which was further amended to 5.0 Ma in the DK section (Deng et al., 2011). The second correlation with GPTS in the DK section indicates that the Phase IV *Hipparion* fauna appeared at ~5.3 Ma within chron. 3r of GPTS (Fig. 9E).

The Phase V *Hipparion* fauna containing the so-called *Proboscidipparion* and *Equus* (*Equus eisenmannae*) (Deng, 2012) was discovered in the lower part of the loess profile of the LD section (Zan et al., 2016) (Fig. 1B). The first paleomagnetic study from the section showed that the Phase V *Hipparion* fauna was approximately 2.5 Ma in age (Qiu et al., 2004), while the subsequent paleomagnetic dating suggested a time interval between 2.2 Ma to 1.9 Ma (Liu et al., 2008). Recent detailed magnetostratigraphic studies for the loess deposits from the two boreholes in the LD section and the NLS section demonstrated that the loess began depositing in the Linxia Basin at 3.0 Ma, and clearly stated that the Phase V *Hipparion* fauna has an age range of 2.5 Ma -

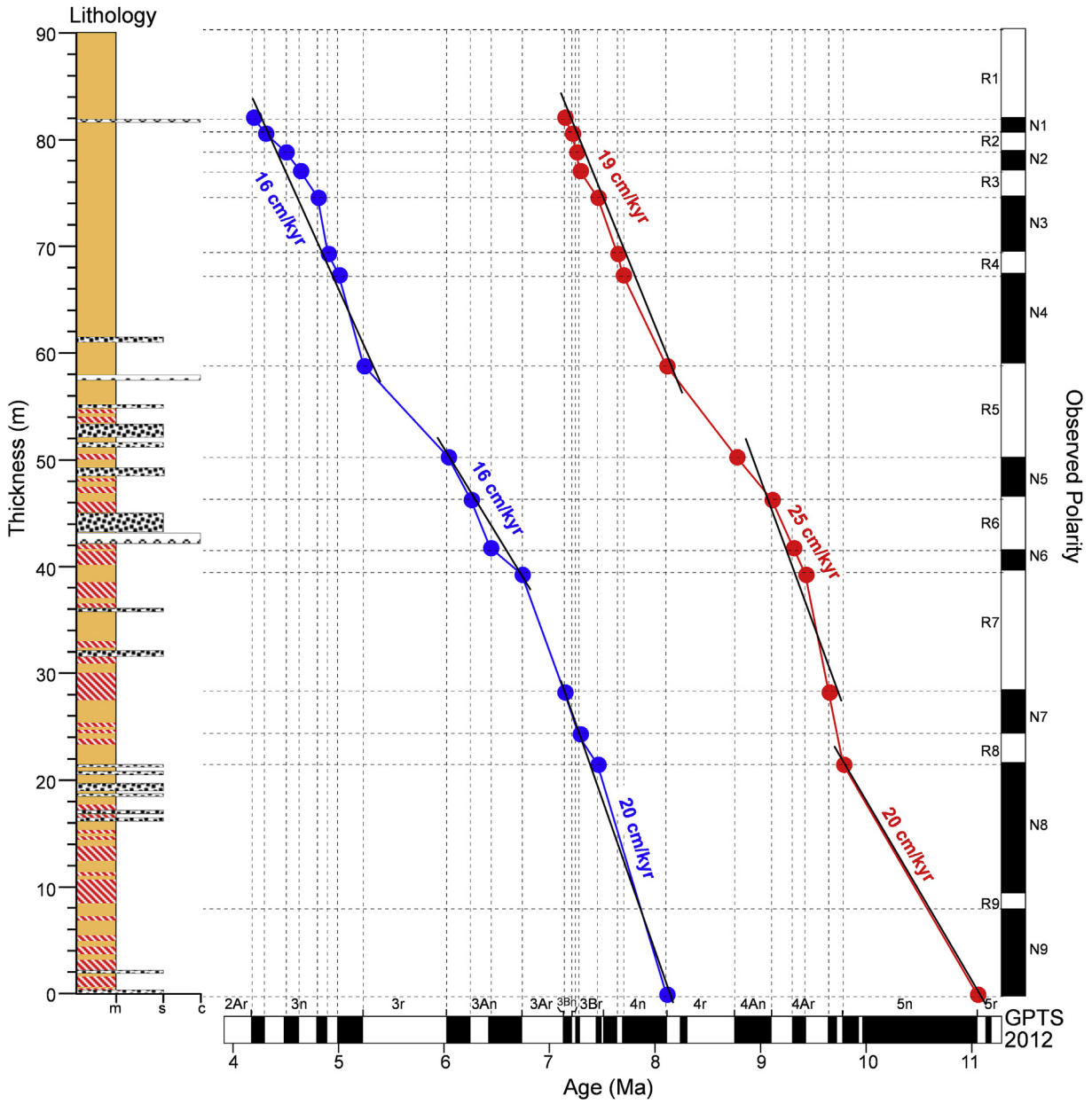

Fig. 8. Stratigraphic thickness vs. magnetostratigraphic age plots of the main magnetic polarity chrons. for the DK section, illustrating changes in sedimentation rates. Red/blue lines are from data of the first/second correlations in Fig. 6. (For interpretation of the references to colour in this figure legend, the reader is referred to the Web version of this article.)

2.2 Ma (Zan et al., 2016, 2018) (Fig. 9A, C). Phase V (2.5 Ma - 2.2 Ma) was the coexisting stages for the *Hipparion* fauna and the *Equus* fauna (Deng, 2012), and the former has a relatively lower evolutional degree than the latter, so during this phase the *Hipparion* such as *Proboscidipparion* was most likely to first appear at 2.5 Ma, and then the following *Equus* emerged in the Linxia Basin (Fig. 9A, C).

6.2. Living environment of the Hipparion fauna from the Linxia Basin

Mammals are extremely sensitive to climatic and environmental changes, and their successions can reflect the aridification of the Asian interior and the evolution of the east Asian monsoon associated with the large uplift of the Tibetan Plateau in the late Cenozoic (Qiu et al., 2013; Fang et al., 2016; Zan et al., 2016). The alternations of four representative mammal faunas (*Dzungariotherium*, *Platybelodon*, *Hipparion* and *Equus*) in the Linxia Basin indicated the gradual deteriorative ecologic environmental changes since the Miocene (Deng et al., 2004, 2013; Qiu et al., 2004; Zhang et al., 2019). An especially significant transition at 11.1 Ma was indicated by the *Platybelodon* fauna, who lived in warm and humid forests, evolving to the *Hipparion*, who lived in warm and subarid steppes (Zhang et al., 2019) (Fig. 10H). After 11.5 Ma, the Linxia Basin entered a brand-new period for the *Hipparion* fauna (Fang et al., 2016; Zhang et al., 2019), as at least seven species of *Hipparion* existed: *H. Dongxiangense, Hipparion* sp., *H. chiai, H. weihoense, H. coelophyes, H. dermatorhinum, and Proboscidipparion* (Deng et al., 2004; Deng, 2012). *Hipparion* had high crowned cheek teeth characterized by a thick chalky covering and complex enamel folds (Fig. 2), which indicate that it was a typical animal feeding on high-fiber and low-moisture herbs (Tong, 2002; Deng et al., 2004) (Fig. 10F). Compared with modern horses, *Hipparion* had slender limbs to adapt to running in a wider open steppe. From the oldest *H. Dongxiangense* at 11.5 Ma to the early Pleistocene *Proboscidipparion* at 2.5 Ma, the *Hipparion* body became gradually tall, the lateral toes of the front and rear hooves became short and thin, and the high-crowned cheek teeth with

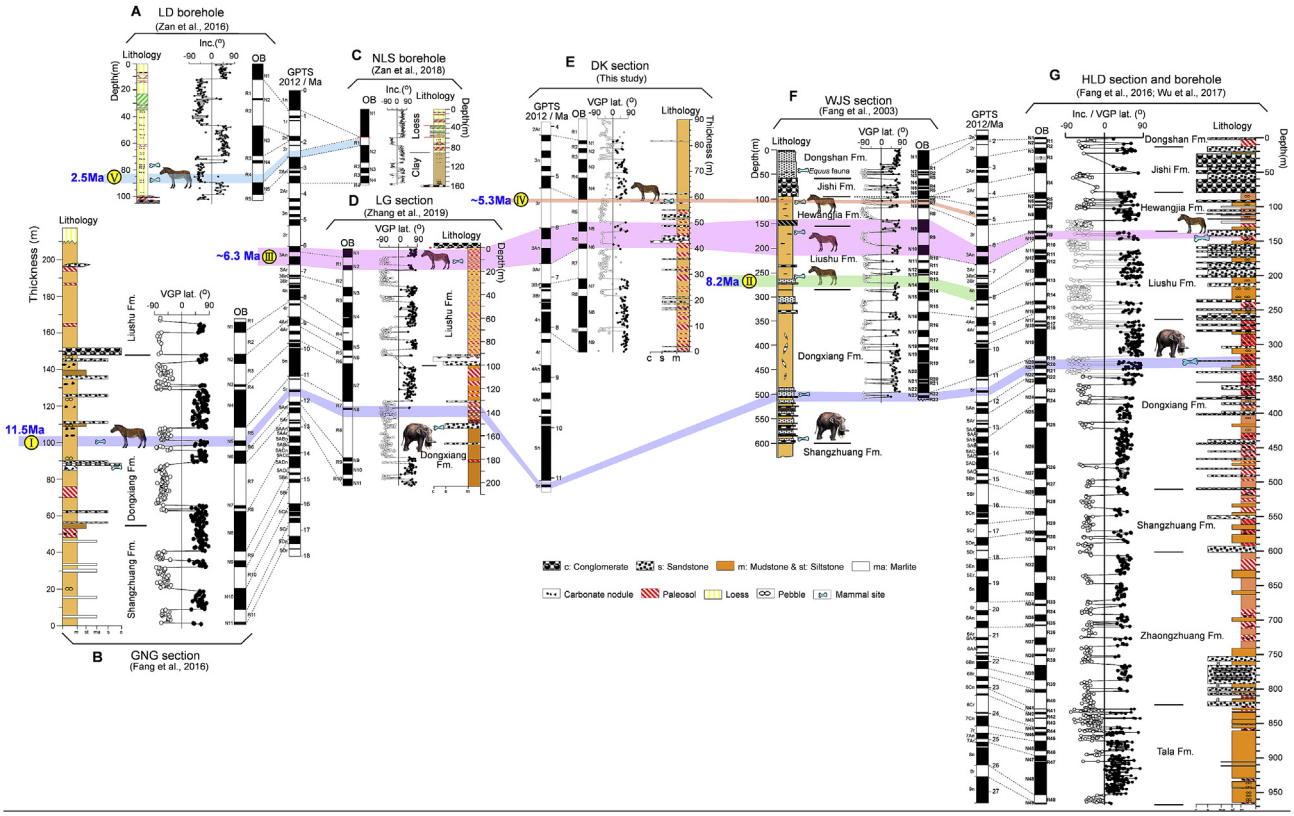

Fig. 9. Magnetostratigraphic contrasts of the sections bearing the *Hipparion* fauna in the Linxia Basin and their correlations with the GPTS of Gradstein et al. (2012). (A) the Longdan borehole (Zan et al., 2016); (B) the Guonigou section (Fang et al., 2016); (C) the Nalesi borehole (Zan et al., 2018); (D) the Laogou section (Zhang et al., 2019); (E–F) the Duikang section from this study; (G) the Wangjiashan section (Fang et al., 2003); (H) the Heilingding section (Fang et al., 2016). GPTS: the geomagnetic polarity time scale; OB: the observed polarity.

the larger chewing face became wider and more complex, revealing that the ecological environment showed stepwise drying and cooling and that the steppe experienced more desertification in the Linxia Basin since the late Miocene. Notably, the body size of the herbivores is critical to determining the affordable ration of fiber/protein in its food (Janis, 1976), and the protein needed by the per unit weight decreases with the increasing weight (Deng et al., 2004), further showing that the later large-sized *Hipparion* may have lived in a steppe environment with cold temperatures and *duriherbosa* vegetation.

The $\delta^{18}O$ from the carbonates in the Linxia Basin implies a trend of increasingly arid conditions at the NE margin of the Tibetan plateau since 12.0 Ma (Dettman et al., 2003) (Fig. 10A). Stepwise aridification in the climate after 12.0 Ma was also confirmed by a progressive decrease of the ratio of arbor to non-arbor trees from pollen records of pollen-spores from the Linxia Basin and Jiuquan Basin (Wu et al., 2004, 2007, 2011; Ma et al., 1998, 2005; Li et al., 2011) (Fig. 10B), the reduced content of broadleaved trees in the regions neighboring the northeastern Tibetan Plateau (Li et al., 2014) (Fig. 10C), the increased *n*-alkanes C_{31}/C_{27} (grasses-shrubs/forests) value on the Loess Plateau (Bai et al., 2009); the gradual increase in the chloride content from the Qaidam Basin indicated the enhancement of aridification (Guo et al., 2018) (Fig. 10D). Meanwhile, the aridification in the Linxia Basin was accompanied by a long-term global cooling inferred by the deep-sea oxygen isotope record after 12 Ma (Zachos et al., 2008) (Fig. 10E), a further expansion of the eastern Antarctic ice-sheet at ~11 Ma, an onset of the western Antarctic ice-sheet at ~8 Ma and an expansion of the north Hemisphere ice sheet at 2.5 Ma (Fig. 10G). Furthermore, the multiple rapid uplifts of the Tibetan Plateau since ~8.0 Ma intensified the Asian winter monsoon at ~8.0 Ma (Quade et al., 1989; Fan et al., 2006; Molnar et al., 2010; Royden et al., 2008; Yang et al., 2017) and further promoted the onset of the loess accumulation on the Loess Plateau at 2.5 Ma (An et al., 2001) (Fig. 10G). Therefore, we suggest that the global cooling and rapid uplift of the plateau resulted in the gradual drying and cooling in the Linxia Basin since the late Miocene, accelerated the desertification of the warm and subarid steppe, and led to the rapid evolution and even the eventual extinction of *Hipparion* at 2.2 Ma.

7. Conclusions

Magnetostratigraphic dating of the sedimentary sequences from the DK section bearing abundant fossils of the *Hipparion* fauna in the Linxia Basin on the NE Tibetan Plateau yields age ranges of approximately 8.1 Ma - 3.7 Ma, and the *Hipparion* fauna bed is dated as being deposited at 5.3 Ma. The combined magnetostratigraphic studies with the ages of *Hipparion* in the Linxia Basin demonstrate that the *Hipparion* fauna mainly lived during five different phases, i.e., 11.5 Ma, 8.2 Ma, 6.3 Ma, 5.3 Ma and 2.5 Ma. The inferred climate in the Linxia Basin and aridification records from its surrounding regions suggest that global cooling and the rapid uplift of the northeastern Tibetan Plateau since the late Miocene jointly triggered the rapid evolution of *Hipparion*.

Declaration of competing interest

We declare that we do not have any academic or associative interest that represents a conflict of interest in connection with our paper submitted.

Acknowledgements

We thank Miao Yunfa, Yan Xiaoli, Pan Meihui, Xu Li, Xia Wenmin, Li Shiyuan, Li Aiyin, Chen Chuanfei and Zhang Qibo for their assistance

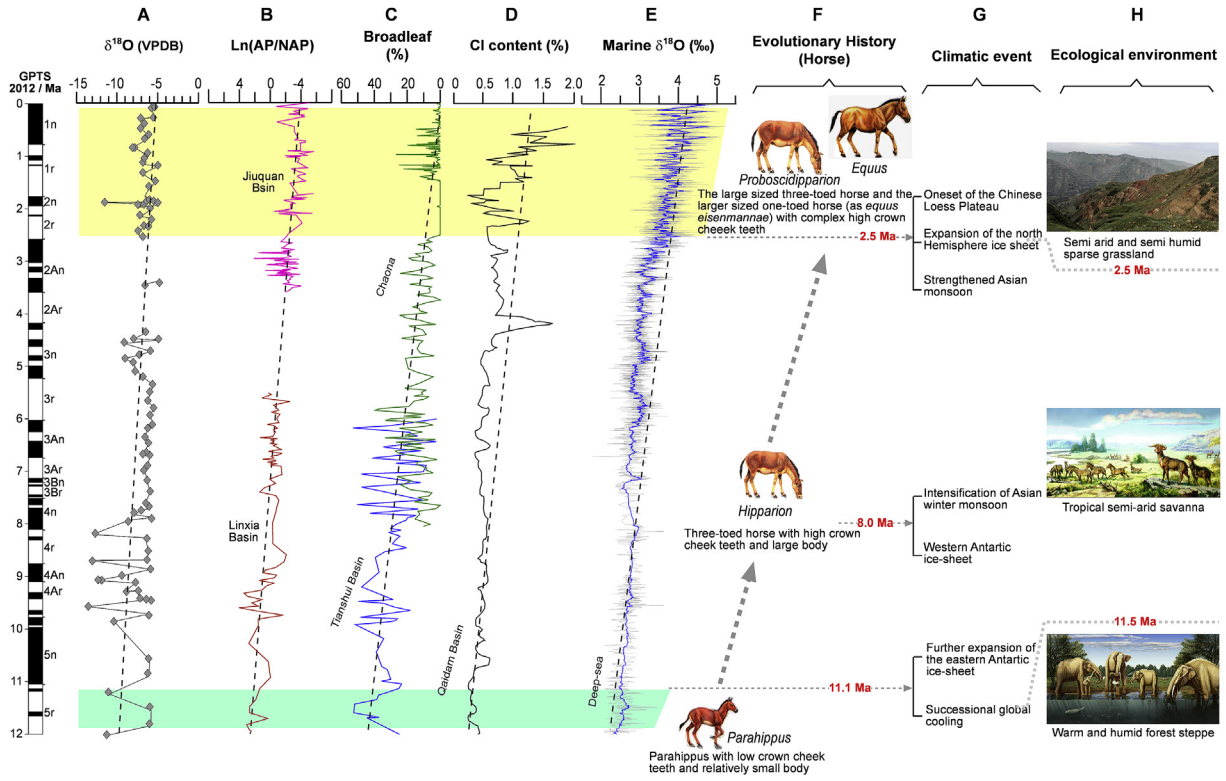

Fig. 10. Comparisons of climate variations and trends with the global and regional climatic events since the late Miocene from $\delta^{18}O$ of the Linxia Basin (Dettman et al., 2003) (A), ratio of arbor to non-arbor trees (AP/NAP) from the Linxia Basin and Jiuquan Basin (Wu et al., 2004, 2007; 2011; Ma et al., 1998, 2005; Li et al., 2011) (B), the content of broadleaved trees from the Tianshui Basin and the Chaona section of the Loess Plateau (C), the chloride content from the Qaidam Basin (Guo et al., 2018) (D), the global oxygen isotope climatic change (Zachos et al., 2008) (E), the evolutionary history of *Hipparion* (Tong, 2002) (F), the global and regional climatic events (Fang et al., 2019; An et al., 2001) (G), the restored ecological environment implied by fossil assemblages (Zhang et al., 2019).

in the field work and Deng Tao and Hou Sukuan for their field recognition of fossil mammal sites. This work is co-supported by the Strategic Priority Research Program of the Chinese Academy of Sciences (Grant XDA20070201), the Second Tibetan Plateau Scientific Expedition and Research (Grant 2019QZKK0707) and the National Natural Science Foundation of China (Grants 41672358, 41620104002).

Appendix A. Supplementary data

Supplementary data to this article can be found online at https://doi.org/10.1016/j.palaeo.2019.109413.

References

An, Z.S., Kutzbach, J.E., Prell, W.L., Porter, S.C., 2001. Evolution of Asian monsoons and phased uplift of the Himalaya-Tibetan plateau since Late Miocene times. Nature 411, 62–66.

Alberdi, M.T., 1989. A review of Old World hipparionine horses. In: Prothero, D.R., Schoch, R.M. (Eds.), The Evolution of Perissodactyls. Oxford University Press, New York, pp. 234–261.

Bernor, R.L., Sun, B.Y., 2015. Morphology through ontogeny of Chinese proboscidipparion and plesiohipparion and observations on their eurasian and african relatives. Vert. PalAsi. 53, 73–92.

Bai, Y., Fang, X.M., Nie, J.S., Wang, Y.L., Wu, F.L., 2009. Paleoecological and paleoclimatic history on the Chinese Loess Plateau recorded by biomarkers: implication for the last 8 Ma Asian drying evolution. Palaeogeogr. Palaeoclimatol. Palaeoecol. 271, 161–169.

Bernor, R.L., Koufos, G.D., Woodburne, M.O., Fortelius, M., 1996. The evolutionary history and biochronology of European and southwest Asian Late Miocene and Pliocene hipparionine horses. In: Bernor, R.L., Fahlbusch, V., Mittmann, H.-W. (Eds.), The Evolution of Western Eurasian Neogene Mammal Faunas. Columbia University Press, New York, pp. 30–338.

Deng, T., 2004. Late Cenozoic environmental changes in the Linxia Basin as indicated by cenograms of fossil mammals. Vert. PalAsi. 42, 45–66.

Deng, T., 2012. A skull of hipparion (proboscidipparion) sinense (perissodactyla, qquidae) from longdan, Dongxiang of northeastern China - addition to the early Pleistocene longdan mammalian fauna. Vert. PalAsi. 50, 74–84.

Deng, T., Hou, S.K., Shi, Q.Q., Chen, S.K., He, W., Chen, S.Q., 2011. Terrestrial miopliocene boundary in the Linxia Basin, gansu, China. Acta Geol. Sin. 85, 452–464 (English edition).

Deng, T., Qiu, Z.X., Wang, B.Y., Wang, X.M., Hou, S.K., 2013a. Late Cenozoic biostratigraphy of the Linxia basin, northwestern China. In: Wang, X.M., Flynn, L.J., Fortelius, M. (Eds.), Fossil Mammals of Asia: Neogene Biostratigraphy and Chronology. Columbia University Press, New York, pp. 243–273.

Deng, T., Hou, S.K., Xie, G.P., Wang, S.Q., Shi, Q.Q., Chen, S.K., Sun, B.Y., Lu, X.K., 2013b. Chronostratigraphic subdivision and correlation of the upper Miocene of the Linxia Basin, gansu, China. J. Stratigr. 37, 417–427.

Deng, T., Hou, S.K., Wang, S.Q., 2019. Neogene integrative stratigraphy and timescale of China. Sci. Chin. 62, 310–323.

Deng, T., Wang, X., Ni, X., Liu, L., 2004. Sequence of the Cenozoicmammalian faunas of the Linxia Basin in Gansu, China. Acta Geol. Sin.-Engl. 78, 8–14.

Deng, T., Wang, X.M., Wang, S.Q., Li, Q., Hou, S.K., 2015. Evolution of the Chinese Neogene mammalian faunas and its relationship to uplift of the Tibetan Plateau. Adv. Earth Sci. 30, 407–415 (in Chinese with English abstract).

Deng, T., Wang, X.M., 2004. Late Miocene hipparion (equidae, mammalia) of eastern Qaidam Basin in qinghai, China. Vert. PalAsi. 42, 316–333.

Dettman, D.L., Fang, X., Garzione, C.N., Li, J.J., 2003. Uplift-driven climate change at 12 Ma: a long δ18O record from the NE margin of the Tibetan Plateau. Earth Planet. Sci. Lett. 214, 267–277.

Fan, M.J., Song, C.H., Dettman, D.L., Fang, X.M., Xu, X.H., 2006. Intensification of the asian winter monsoon after 7.4Ma: grain-size evidence from the Linxia Basin, northeastern Tibetan plateau, 13.1 Ma to 4.3 Ma. Earth Planet. Sci. Lett. 248, 171–182.

Fang, X.M., Fang, Y.H., Zan, J.B., Zhang, W.L., Song, C.H., Appel, E., Meng, Q.Q., Miao, Y.F., Dai, S., Lu, Y., Zhang, T., 2019. Cenozoic magnetostratigraphy of the Xining Basin, NE Tibetan Plateau, and its constraints on paleontological, sedimentological and tectonomorphological evolution. Earth Sci. Rev. 190, 460–485.

Fang, X.M., Li, J.J., Zhu, J.J., Chen, H.L., Cao, J.X., 1997. Division and age dating of the cenozoic strata of the Linxia Basin in gansu, China. Chin. Sci. Bull. 42, 1457–1471 (in Chinese).

Fang, X.M., Garzione, C., Van der Voo, R., Li, J.J., Fan, M.J., 2003. Flexural subsidence by 29 Ma on the NE edge of tibet from the magnetostratigraphy of Linxia Basin, China. Earth Planet. Sci. Lett. 210, 545–560.

Fang, X.M., Wang, J.Y., Zhang, W.L., Zan, J.B., Song, C.H., Yan, M.D., Appel, E., 2016. Tectonosedimentary evolution model of an intracontinental flexural (foreland) basin for paleoclimatic research. Glob. Planet. Chang. 145, 78–97.

Gradstein, F., Ogg, J., Schmitz, M., Ogg, G., 2012. The Geologic Time Scale 2012. Elsevier.
Gu, Z.G., Wang, S.H., Hu, S.Y., Wei, D.T., 1995. Research progress on biostratigraphy of tertiary red beds in Linxia Basin, gansu province. Study on the Formation and Evolution of the Qinghai-Xizang Plateau, Environmental Change and Ecological System. Science Press, Beijing, pp. 91–95.
Guo, P., Liu, C.Y., Huang, L., Yu, M.L., Wang, P., Zhang, G.Q., 2018. Palaeohydrological evolution of the late Cenozoic saline lake in the Qaidam Basin, NE Tibetan Plateau: tectonic vs. climatic control. Glob. Planet. Chang. 165, 44–61.
Guo, Z.T., Ruddiman, W.F., Hao, Q.Z., Wu, H.B., Qiao, Y.S., Zhu, R.X., Peng, S.Z., Wei, J.J., Yuan, B.Y., Liu, T.S., 2002. Onset of Asian desertification by 22 Myr ago inferred from loess deposits in China. Nature 416, 159–163.
Hao, Q.Z., Guo, Z.T., 2004. Magnetostratigraphy of a late Miocene-Pliocene loess-soil sequence in the western Loess Plateau in China. Geophys. Res. Lett. L09209. https://doi.org/10.1029/2003GL019392.
Janis, C.M., 1976. The evolutionary strategy of the Equidae and the origins of rumen and cecal digestion. Evolution 30, 757–774.
Li, J.J., et al., 1995. Uplift of Qinghai-Xizang (Tibet) Plateau and Global Change. Lanzhou university Press, Lanzhou.
Li, J.J., Fang, X.M., Song, C.H., Pan, B.T., Ma, Y.Z., Yan, M.D., 2014. Late Miocene-Quaternary rapid stepwise uplift of the NE Tibetan Plateau and its effects on climatic and environmental changes. Quat. Res. 81 (3), 400–423.
Li, J.J., Fang, X.M., Van der Voo, R., Zhu, J.J., MacNiocaill, C., Cao, J.X., Zhong, W., Chen, H.L., Wang, J.L., Wang, J.M., 1997. Late cenozoic magnetostratigraphy (11 - 0 Ma) of the dongshanding and wangjiashan sections in the longzhong basin, western China. Geol. Mijnb. 76, 121–134.
Li, X.R., Fang, X.M., Wu, F.L., Miao, Y.F., 2011. Pollen evidence from baode of the northern Loess Plateau of China and strong east Asian summer monsoons during the early Pliocene. Chin. Sci. Bull. 56, 64–69.
Liu, P., Zhang, S., Han, J.M., Liu, T.S., 2008. Paleomagnetic chronology of quaternary stratigraphy of the Longdan section in Gansu province of China. Quat. Sci. 28, 796–805 (in Chinese with English abstract).
Ma, Y.Z., Li, J.J., Fang, X.M., 1998. Pollen-spores in the red bed during 30.6-5 Ma in the Linxia Basin and climatic evolution. Chin. Sci. Bull. 43, 301–304 (in Chinese).
Ma, Y.Z., Fang, X.M., Li, J.J., Wu, F.L., Zhang, J., 2005. The vegetation and climate change during neocene and early quaternary in jiuxi basin. Sci. China Ser. D Earth Sci. 48, 676–688.
Macfadden, B.J., 1984. Systematics and phylogeny of hipparion, neohipparion, nannipus and cormohipparion (mammalia, equidae) from the Miocene and Pliocene of the new World. Bull. Am. Mus. Nat. Hist. 179, 1–95.
McFadden, P.L., McElhinny, M.W., 1990. Classification of the reversal test in paleomagnetism. Geophys. J. Int. 103, 725–729.
Molnar, P., Boos, W.R., Battisti, D.S., 2010. Orographic controls on climate and paleoclimate of Asia: thermal and mechanical roles for the Tibetan Plateau. Annu. Rev. Earth Planet Sci. 38, 77–102.
Qiu, Z.X., Deng, T., Wang, B.Y., 2004. Early Pleistocene Mammalian Fauna fromLongdan, Dongxiang, Gansu, China. Science Press, Beijing, pp. 1–156.
Qiu, Z.X., Huang, W.L., Guo, Z.H., 1987. The Chinese Hipparionine fossils. Palaeontologia Sinica, New Ser C 25, 1–250 (in Chinese with English summary).
Qiu, Z.X., Qiu, Z.D., 1990. Neogene local mammalian f aunas :succession and ages. J. Stratigr. 14, 241–260 (in Chinese).
Qiu, Z.X., Qiu, Z.D., Deng, T., Li, C.K., Zhang, Z.Q., Wang, B.Y., Wang, X.M., 2013. Neogene land mammal stages/ages of China. In: Wang, X.M., Flynn, L.J., Fortelius, M. (Eds.), Fossil Mammals of Asia: Neogene Biostratigraphy and Chronology. Columbia University Press, New York, pp. 29–90.
Qiu, Z.X., Wu, W.Y., Qiu, Z.D., 1999. Miocene mammal faunal sequence of China: palaeozoogeography and Eurasian relationships. In: Rössner, G.E., Heissig, K. (Eds.), The Miocene Land Mammals of Europe. München. Verlag Dr. Friedrich Pfeil, pp. 443–455.
Quade, J., Cerling, T.E., Bowman, J.R., 1989. Development of Asian Monsoon revealed by mark ecological shift during the latest Miocene in Northern Pakistan. Nature 342, 163–166.
Royden, L.H., Burchfiel, B.C., van der Hilst, R.D., 2008. The geological evolution of the Tibetan Plateau. Science 321, 1054–1058.
Steininger, F.F., 1999. Chronostratigraphy, geochronology and biochronology of the Miocene "european land mammal mega-zones" (ELMMZ) and the Miocene "Mammal-Zones (MN-Zones)". In: Rössner, G.E., Heissig, K. (Eds.), The Miocene Land Mammals of Europe. München. Verlag Dr. Friedrich Pfeil, pp. 9–24.
Tauxe, L., 1998. Paleomagnetic Principles and Practice. Kluwer Academic Publishers, Dordrecht, pp. 299.
Tong, H.W., 2002. Evolution of horses. Fossil 1, 2–4 (in Chinese).
Wang, J.Y., Fang, X.M., Zhang, W.L., Zan, J.B., Miao, Y.F., Li, S.Y., 2010. Magnetostratigraphy and implications of the Heilinding section, the Linxia basin, Gansu province, China. Mar. Geol. Quat. Geol. 30 (5), 129–135 (in Chinese with English abstract).
Wang, X.M., Flynn, L.J., Fortelius, M., 2013. Fossil Mammals of Asia: Neogene Biostratigraphy and Chronology. Columbia University Press, New York.
Woodburne, M.O., Swisher, III.C.C., 1995. Land mammal high-resolution geochronology, intercontinental overland dispersal, sea level, climate, and vicariance. Society of Economic Paleontologists and Mineralogists, Spec. Publ. 54, 335–364.
Wu, F.L., Fang, X.M., Ma, Y.Z., An, Z.S., Li, J.J., 2004. A 1.5 Ma sporopollen record of paleoecologic environment evolution in the central Chinese Loess Plateau. Chin. Sci. Bull. 49, 295–301.
Wu, F.L., Fang, X.M., Ma, Y.Z., Herrmann, M., Mosbrugger, V., An, Z.S., Miao, Y.F., 2007. Plio-Quaternary stepwise drying of Asia: evidence from a 3-Ma sporopollen record from the Chinese Loess Plateau. Earth Planet. Sci. Lett. 257, 160–169.
Wu, F.L., Fang, X.M., Herrmann, M., Mosbrugger, V., Miao, Y.F., 2011. Extended drought in the interior of Central Asia since the Pliocene reconstructed fromsporopollen records. Glob. Planet. Chang. 76, 16–21.
Wu, F.L., Fang, X.M., Meng, Q.Q., Zhao, Y., Tang, F.J., Zhang, T., Zhang, W.L., Zan, J.B., 2017. Magneto- and litho-stratigraphic records of the oligocene-early Miocene climatic changes from deep drilling in the Linxia Basin, northeast Tibetan plateau. Glob. Planet. Chang. 158, 36–46.
Yang, Y.B., Galy, A., Fang, X.M., Yang, R.S., Zhang, W.L., Zan, J.B., 2017. Eolian dust forcing of river chemistry on the northeastern Tibetan Plateau since 8Ma. Earth Planet. Sci. Lett. 464, 200–210.
Zachos, J.C., Gerald, R.D., Richard, E.Z., 2008. An early Cenozoic perspective on greenhouse: warming and carbon-cycle dynamics. Nature 451 (17), 279–283.
Zan, J.B., Fang, X.M., Zhang, W.L., Yan, M.D., Zhang, T., 2016. Palaeoenvironmental and chronological constraints on the Early Pleistocene mammal fauna from loess deposits in the Linxia Basin, NE Tibetan Plateau. Quat. Sci. Rev. 148, 234–242.
Zan, J.B., Fang, X.M., Zhang, W.L., Yan, M.D., Zhang, D.W., 2018. A new record of late Pliocene-early Pleistocene aeolian loess-red clay deposits from the western Chinese Loess Plateau and its palaeoenvironmental implications. Quat. Sci. Rev. 186, 17–26.
Zhang, W.L., Appel, E., Wang, J.Y., Fang, X.M., Zan, J.B., Yang, Y.B., Miao, Y.F., Yan, X.L., 2019. New paleomagnetic constraints for Platybelodon and Hipparion faunas in the Linxia Basin and their ecological environmental implications. Glob. Planet. Chang. 176, 71–83.